

Semileptonic decays of doubly charmed baryons with bag model

Chao-Qiang Geng, Chia-Wei Liu, Aowen Zhou and Xiao Yu

School of Fundamental Physics and Mathematical Sciences,

Hangzhou Institute for Advanced Study, UCAS, Hangzhou 310024, China

University of Chinese Academy of Sciences, 100190 Beijing, China

(Dated: November 9, 2022)

Abstract

We study the semileptonic decays of $B_{cc} \rightarrow B_c \ell^+ \nu_\ell$ with the bag model, where $\ell = (e, \mu)$, $B_{cc} = (\Xi_{cc}^{++}, \Xi_{cc}^+, \Omega_{cc}^+)$, and B_c are the singly charmed baryons with $J^P = 1/2^+$. We obtain the decay widths of $\Gamma(\Xi_{cc}^{++} \rightarrow \Xi_c^+ e^+ \nu_e, \Xi_c'^+ e^+ \nu_e, \Lambda_c^+ e^+ \nu_e, \Omega_c^+ e^+ \nu_e) = (5.1 \pm 0.1, 11 \pm 1, 0.34 \pm 0.06, 0.76 \pm 0.06) \times 10^{-14}$ GeV, $\Gamma(\Xi_{cc}^+ \rightarrow \Xi_c^0 e^+ \nu_e, \Xi_c'^0 e^+ \nu_e, \Sigma_c^0 e^+ \nu_e) = (5.1 \pm 0.6, 11 \pm 1, 1.5 \pm 0.1) \times 10^{-14}$ GeV, and $\Gamma(\Omega_{cc}^+ \rightarrow \Omega_c^0 e^+ \nu_e, \Xi_c^0 e^+ \nu_e, \Xi_c'^0 e^+ \nu_e) = (22 \pm 2, 0.32 \pm 0.04, 0.77 \pm 0.06) \times 10^{-14}$ GeV. We also get that $\Gamma(B_{cc} \rightarrow B_c \mu^+ \nu_\mu) / \Gamma(B_{cc} \rightarrow B_c e^+ \nu_e) = 0.97 \sim 1.00$. In addition, we discuss the $SU(3)$ flavor breaking effects, classified into three aspects: phase space differences, spectator quarks, and overlappings of the transited quarks. In particular, we show that the breaking effects are dominated by the phase space differences, which can be as large as 25%. Explicitly, we find that $\Gamma(\Xi_{cc}^{++} \rightarrow \Lambda_c^+ e^+ \nu_e) V_{cs}^2 / \Gamma(\Xi_{cc}^{++} \rightarrow \Xi_c^+ e^+ \nu_e) V_{cd}^2 = 1.24$, which is expected as 1 under the exact $SU(3)$ flavor symmetry.

I. INTRODUCTION

In 2002, the SELEX collaboration reported a resonant structure in $\Lambda_c^+ K^- \pi^+$ and $p D^+ K^-$ [1, 2], which can be potentially caused by $\Xi_{cc}^+(3620)$. However, the same structure was not confirmed by the FOCUS, BABAR and BELLE collaborations [3–5]. Eventually, the long awaited evidence finally arrived in 2017 via $\Xi_{cc}^{++} \rightarrow \Lambda_c^+ K^- \pi^+ \pi^+$ at LHCb [6], where the mass is determined to be

$$M_{\Xi_{cc}^{++}} = (3621.40 \pm 0.72 \pm 0.27 \pm 0.14) \text{ MeV}. \quad (1)$$

This encouraging finding was soon accompanied by the lifetime measurement of Ξ_{cc}^{++} [7] as well as the observation of $\Xi_{cc}^{++} \rightarrow \Xi_c^+ \pi^+$ [8]. One can reasonably expect much more experimental results in the future, providing opportunities to deepen our knowledge of hadron physics.

On the theoretical aspect, the low-lying charmed baryons are categorized by the representations of the flavor $SU(3)$ ($SU(3)_F$) symmetry, given in FIG. 1. Under $SU(3)_F$, the doubly charmed baryons (B_{cc}) form a triplet, while the singly charmed baryons (B_c) consist of a antitriplet and a sextet. To deal with the weak decays of B_{cc} , lots of approaches have been performed [9–46]. In the diquark approach, two of the three quarks are grouped as a diquark cluster, simplifying the problem to a two-body one [42–47]. Nonetheless, it is unclear which quarks shall form a diquark cluster. On the other hand, the problem does not exist in the MIT bag model (MBM), as a diquark cluster is unnecessary.

The MBM describes hadrons at rest as localized objects. Along with the bag and zero point energies, the model is suitable to explain the mass spectra. However, it becomes problematic in the decays due to the unwanted center-of-mass motion. This problem can be understood by the Heisenberg uncertainty principle, which states that a localized object can not possess a definite momentum. If we treat a bag state as a baryon at rest, the calculations will not respect the energy-momentum conservation. The problem was tackled a few years ago by taking the linear superposition of infinite bags in Ref [48]. This approach has been applied to various decay systems [49–53].

This paper is organized as follows. We present the formalism of the decay branching fractions in terms of the helicity amplitudes in Sec. II. In Sec. III, we give our numerical results and compare them with those in the literature. We summarize this work in Sec. IV.

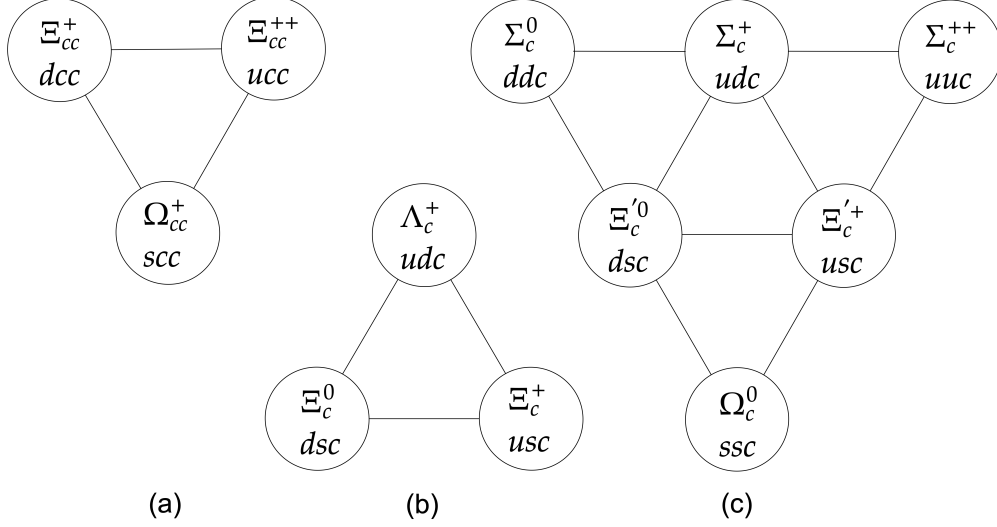


FIG. 1: Quark states of the charmed baryons, where (a) represents an $SU(3)_F$ triplet with the doubly charmed baryons, while (b) and (c) correspond to the $SU(3)_F$ antitriplet and sextet with the singly charmed baryons, respectively.

II. FORMALISM

The effective Hamiltonian for the transitions of $c \rightarrow f\ell^+\nu$ ($f = d, s$) at the quark level is given as

$$\mathcal{H}_{eff} = \frac{G_F}{\sqrt{2}} V_{cf} \bar{\ell} \gamma^\mu (1 - \gamma_5) \nu_\ell \bar{f} \gamma_\mu (1 - \gamma_5) c, \quad (2)$$

where G_F is the Fermi constant, and V_{cf} correspond to the Cabibbo-Kobayashi-Maskawa matrix elements. The weak transition amplitudes of the doubly charmed baryons are then given as

$$\mathcal{A}(B_{cc} \rightarrow B_c \ell^+ \nu_\ell) = \frac{G_F}{\sqrt{2}} V_{cq} \bar{\ell} \gamma^\mu (1 - \gamma_5) \nu_\ell \langle B_c, p_f | \bar{f} \gamma_\mu (1 - \gamma_5) c | B_{cc}, p_i \rangle, \quad (3)$$

with the baryon matrix elements parameterized by

$$\begin{aligned} & \langle B_c, p_f, \lambda_f | \bar{f} \gamma_\mu (1 - \gamma_5) c | B_{cc}, p_i, \lambda_i \rangle \\ &= \bar{u}_f(p_f, \lambda_f) \left[\gamma_\mu f_1(q^2) - i \sigma_{\mu\nu} \frac{q^\nu}{M_i} f_2(q^2) + f_3(q^2) \frac{q_\mu}{M_i} \right] u_i(p_i, \lambda_i) \\ & - \bar{u}_f(p_f, \lambda_f) \left[\gamma_\mu g_1(q^2) - i \sigma_{\mu\nu} \frac{q^\nu}{M_i} g_2(q^2) + g_3(q^2) \frac{q_\mu}{M_i} \right] \gamma_5 u_i(p_i, \lambda_i), \end{aligned} \quad (4)$$

where $f_{123}(q^2)$ and $g_{123}(q^2)$ are the form factors, $\sigma^{\mu\nu} = i[\gamma^\mu, \gamma^\nu]/2$, $q_\mu = p_i^\mu - p_f^\mu$, and $\lambda_{f(i)}$, $p_{f(i)}^\mu$, $M_{f(i)}$ and $u_{f(i)}$ are the helicity, four-momentum, mass and Dirac spinor of $B_{c(i)}$,

respectively.

In order to calculate the decay widths, we introduce a set of helicity amplitudes $H_{\lambda_f \lambda_W}^{V(A)}$, where λ_f and λ_W represent the helicity quantum numbers of B_c and the off-shell W^+ boson, respectively. Relations between the helicity amplitudes and form factors are given by [54]

$$\begin{aligned}
H_{\frac{1}{2}1}^V &= \sqrt{2Q_-} \left(-f_1(q^2) - \frac{M_i + M_f}{M_i} f_2(q^2) \right), \\
H_{\frac{1}{2}0}^V &= \frac{\sqrt{Q_-}}{q^2} \left((M_i + M_f) f_1(q^2) + \frac{q^2}{M_i} f_2(q^2) \right), \\
H_{\frac{1}{2}t}^V &= \frac{\sqrt{Q_+}}{q^2} \left((M_i - M_f) f_1(q^2) + \frac{q^2}{M_i} f_3(q^2) \right), \\
H_{\frac{1}{2}1}^A &= \sqrt{2Q_+} \left(g_1(q^2) - \frac{M_i - M_f}{M_i} g_2(q^2) \right), \\
H_{\frac{1}{2}0}^A &= \frac{\sqrt{Q_+}}{q^2} \left(-(M_i - M_f) g_1(q^2) + \frac{q^2}{M_i} g_2(q^2) \right), \\
H_{\frac{1}{2}t}^A &= \frac{\sqrt{Q_-}}{q^2} \left(-(M_i + M_f) g_1(q^2) + \frac{q^2}{M_i} g_3(q^2) \right),
\end{aligned} \tag{5}$$

where $Q_{\pm} = (M_i \pm M_f)^2 - q^2$ and $H_{\lambda_f \lambda_W}^{V(A)} = (-)H_{-\lambda_f -\lambda_W}^{V(A)}$. The differential decay widths are given in terms of the helicity amplitudes as [54–56]

$$\begin{aligned}
\partial_q \Gamma &= \frac{\partial \Gamma}{\partial q^2} = \frac{1}{3} \frac{G_F^2}{(2\pi)^3} |V_{fc}|^2 \frac{(q^2 - m_\ell^2)^2 p}{8M_i^2 q^2} \left[\left(1 + \frac{m_\ell^2}{2q^2} \right) \right. \\
&\quad \left. \left(|H_{\frac{1}{2}1}^V|^2 + |H_{-\frac{1}{2}1}^V|^2 + |H_{\frac{1}{2}0}^V|^2 + |H_{-\frac{1}{2}0}^V|^2 \right) + \frac{3m_\ell^2}{2q^2} \left(|H_{\frac{1}{2}t}^V|^2 + |H_{-\frac{1}{2}t}^V|^2 \right) \right],
\end{aligned} \tag{6}$$

where $p = \sqrt{Q^+ Q^-} / 2M_{B_i}$, $H_{\lambda_f \lambda_W} = H_{\lambda_f \lambda_W}^V - H_{\lambda_f \lambda_W}^A$ and m_ℓ is the lepton mass.

In this work, we evaluate the form factors with the homogeneous bag model (HBM) [53]. The baryon wave functions of B_{cc} are given as

$$|B_{cc}, \uparrow\rangle = \int \frac{1}{2\sqrt{3}} \epsilon^{\alpha\beta\gamma} q_{a\alpha}^\dagger(\vec{x}_1) c_{b\beta}^\dagger(\vec{x}_2) c_{c\gamma}^\dagger(\vec{x}_3) \Psi_{A_\uparrow}^{abc}(\vec{x}_1, \vec{x}_2, \vec{x}_3) [d^3 \vec{x}] |0\rangle, \tag{7}$$

where $q' = (u, d, s)$ for $B_{cc} = (\Xi_{cc}^{++}, \Xi_{cc}^+, \Omega_{cc}^+)$, q'^\dagger and c^\dagger represent the creation operators of quarks, the Latin and Greek letters stand for the Dirac spinor and color indices, and Ψ_A are the spatial wave functions defined in Refs. [51–53], respectively. On the other hand, the wave functions of B_c can be found in Ref. [51].

We choose the Breit frame to calculate the baryon matrix elements, where B_c and B_{cc} have the opposite velocities $\vec{v} = v\hat{z}$ and $-\vec{v}$. The baryon matrix elements of the current

operators are then governed by

$$\begin{aligned}
\langle B_c(\vec{v}), \lambda_f | f^\dagger \Upsilon c(0) | B_{cc}(-\vec{v}), \lambda_i \rangle &= \mathcal{N}_{B_c} \mathcal{N}_{B_{cc}} \int d^3 \vec{x}_\Delta \Upsilon_{fc}^{\lambda_f \lambda_i}(\vec{x}_\Delta) \prod_{q=c,q'} D_q^v(\vec{x}_\Delta), \\
D_q^v(\vec{x}_\Delta) &= \frac{1}{\gamma} \int d^3 \vec{x} \phi_q^\dagger \left(\vec{x} + \frac{1}{2} \vec{x}_\Delta \right) \phi_q \left(\vec{x} - \frac{1}{2} \vec{x}_\Delta \right) e^{-2iE_q v z}, \\
\Upsilon_{fc}^{\lambda_f \lambda_i}(\vec{x}_\Delta) &= \sum_{\lambda_q \lambda_c} N_{\lambda_q \lambda_c}^{\lambda_f \lambda_i} \int d^3 \vec{x} \phi_{f\lambda_q}^\dagger(\vec{x}^+) S_{\vec{v}} \Upsilon S_{-\vec{v}} \phi_{c\lambda_c}(\vec{x}^-) e^{2i(E_{q'} + E_c) \vec{v} \cdot \vec{x}},
\end{aligned} \tag{8}$$

where $\mathcal{N}_{B_c, B_{cc}}$ are the normalization constants, Υ is an arbitrary Dirac matrix, $\vec{x}^\pm = \vec{x} \pm \vec{x}_\Delta/2$, ϕ_q are the bag wave functions in the MBM, $S_{\pm v} = a_\pm \pm a_- \gamma^0 \gamma^3$ with $a_\pm = \sqrt{1 \pm \gamma^2}$ and $\gamma = 1/\sqrt{1 - v^2}$, and $\lambda_{q,c} \in \{\uparrow, \downarrow\}$. The derivations of Eq. (8) and the explicit forms of ϕ_q are given in Ref. [53]. The first line of Eq. (8) is the total overlapping between B_{cc} and B_c induced by $f^\dagger \Upsilon c(0)$ at the quark level, while the second and third terms are interpreted as :

- The spectator quark effects are governed by $D_q^v(\vec{x}_\Delta)$, which describe the overlapping of q in two bag states separated by \vec{x}_Δ .
- The quark transitions are described by $\Upsilon_{fc}^{\lambda_f \lambda_i}$, where $N_{\lambda_q \lambda_c}^{\lambda_f \lambda_i}$ are the spin-flavor overlapping coefficients.

In the heavy constituent quark limit ($m_{u,d,c} \rightarrow \infty$), the formalism is reduced to

$$\begin{aligned}
\langle B_c(\vec{v}), \uparrow | f^\dagger c(0) | B_{cc}(-\vec{v}), \uparrow \rangle &= \sum_{\lambda_q \lambda_c} N_{\lambda_q \lambda_c}^{\uparrow \uparrow}, \\
\langle B_c(\vec{v}), \uparrow | f^\dagger \gamma^0 \gamma^1 \gamma_5 c(0) | B_{cc}(-\vec{v}), \downarrow \rangle &= \sum_{\lambda_q \lambda_c} N_{\lambda_q \lambda_c}^{\uparrow \downarrow}.
\end{aligned} \tag{9}$$

From the angular momentum conservation, we have that

$$N_{\lambda_q \lambda_c}^{\lambda_f \lambda_i} = 0 \quad \text{for } \lambda_f - \lambda_i \neq \lambda_c - \lambda_q. \tag{10}$$

It states that if the baryon spin is (un)flipped by the operator, then the spin of the quark shall also be (un)flipped. In addition, by the Wigner-Eckart theorem, we find that

$$N_{\lambda_q \lambda_c}^{\uparrow \uparrow} = N_{-\lambda_q - \lambda_c}^{\downarrow \downarrow}, \quad N_{\uparrow \uparrow}^{\uparrow \uparrow} - N_{\downarrow \downarrow}^{\uparrow \uparrow} = N_{\downarrow \uparrow}^{\downarrow \uparrow} = N_{\uparrow \downarrow}^{\downarrow \uparrow}. \tag{11}$$

Consequently, there are only two independent numbers given as

$$N_{\text{unflip}} \equiv N_{\uparrow \uparrow}^{\uparrow \uparrow} + N_{\downarrow \downarrow}^{\uparrow \uparrow}, \quad N_{\text{flip}} \equiv N_{\downarrow \uparrow}^{\downarrow \uparrow}, \tag{12}$$

which are collected in TABLE I.

TABLE I: The spin-flavor overlappings of $B_{cc} \rightarrow B_c$.

$c \rightarrow s$	N_{unflip}	N_{flip}	$c \rightarrow d$	N_{unflip}	N_{flip}
$\Xi_{cc}^{++} \rightarrow \Xi_c^+$	$\frac{\sqrt{6}}{2}$	$\frac{\sqrt{6}}{6}$	$\Xi_{cc}^{++} \rightarrow \Lambda_c^+$	$\frac{\sqrt{6}}{2}$	$\frac{\sqrt{6}}{6}$
$\Xi_{cc}^+ \rightarrow \Xi_c^0$	$\frac{\sqrt{6}}{2}$	$\frac{\sqrt{6}}{6}$	$\Omega_{cc}^+ \rightarrow \Xi_c^0$	$\frac{\sqrt{6}}{2}$	$\frac{\sqrt{6}}{6}$
$\Xi_{cc}^{++} \rightarrow \Xi_c'^+$	$-\frac{\sqrt{2}}{2}$	$-\frac{5\sqrt{2}}{6}$	$\Xi_{cc}^{++} \rightarrow \Sigma_c^+$	$-\frac{\sqrt{2}}{2}$	$-\frac{5\sqrt{2}}{6}$
$\Xi_{cc}^+ \rightarrow \Xi_c'^0$	$-\frac{\sqrt{2}}{2}$	$-\frac{5\sqrt{2}}{6}$	$\Omega_{cc}^+ \rightarrow \Xi_c'^0$	$-\frac{\sqrt{2}}{2}$	$-\frac{5\sqrt{2}}{6}$
$\Omega_{cc}^+ \rightarrow \Omega_c^0$	-1	$-\frac{5}{3}$	$\Xi_{cc}^+ \rightarrow \Sigma_c^0$	-1	$-\frac{5}{3}$

III. NUMERICAL RESULTS

The values of V_{cf} are given by [57]

$$|V_{cs}| = 0.987 \pm 0.011, \quad |V_{cd}| = 0.221 \pm 0.004, \quad (13)$$

while the model parameters are taken as [53]

$$R = 4.7 \pm 0.3 \text{ GeV}^{-1}, \quad m_c = 1.655 \text{ GeV}, \quad m_{u,d} = 0, \quad m_s = 0.2 \pm 0.1 \text{ GeV}. \quad (14)$$

Notice that B_{cc} and B_c have different bag radii, found to be around 4.4 and 5.0 GeV^{-1} , respectively [58]. However, to simplify the formalism, we take their bag radii as equal and allow them to vary from 4.4 to 5.0 GeV^{-1} .

To illustrate the recoil effects of the form factors, we plot those of $\Omega_{cc}^+ \rightarrow \Omega_c$ in FIG. 2. We define

$$\omega \equiv \frac{M_i^2 + M_f^2 - q^2}{2M_i M_f} = \frac{1 + v^2}{1 - v^2}, \quad (15)$$

so that the zero recoil point ($q^2 = q_{max}^2 = (M_i - M_f)^2$) corresponds to $\omega = 1$ for all the decays. As shown in the figures, f_3 and g_2 can be taken as zero practically. The uncertainties of f_1 and g_1 are negligible at the low q^2 regions, and around 10% at $\omega = 1.06$. As a result, at $\omega = 1$, f_1 and g_1 are not polluted by the uncertainties of the quark energies. However, the uncertainties of f_2 and g_3 are large in all regions.

The form factors of $\Xi_{cc}^{++} \rightarrow B_c$ at $q^2 = 0$, along with those in the literature, are given in Table II. For completeness, we also show all our calculated values of the form factors for $\Xi_{cc}^{++} \rightarrow B_c$ with the HBM in Table III. Note that the form factors of $\Xi_{cc}^{++} \rightarrow \Xi_c^+$ and $\Xi_{cc}^+ \rightarrow \Xi_c^0$ are the same due to the isospin symmetry. Compared to those in the literature,

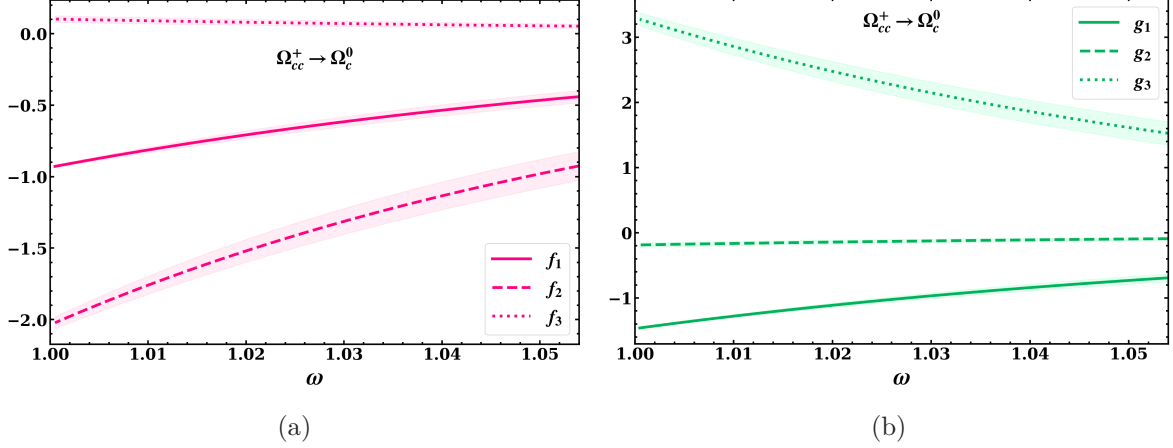


FIG. 2: The form factors of $\Omega_{cc}^+ \rightarrow \Omega_c$ as functions of ω , where the central lines and bands correspond to the central values and uncertainties, respectively.

TABLE II: The form factors of Ξ_{cc}^{++} calculated in the HBM, light-front quark model (LFQM), and QCD sum rule (QCDSR) at $q^2 = 0$.

	HBM (This work)	LFQM [11, 41]	QCDSR [38, 40, 41]
$f_1^{\Xi_{cc}^{++} \rightarrow \Lambda_c^+}$	0.28 ± 0.05	-0.79	-0.59 ± 0.05
$f_2^{\Xi_{cc}^{++} \rightarrow \Lambda_c^+}$	-0.01 ± 0.01	0.008	0.039 ± 0.024
$f_3^{\Xi_{cc}^{++} \rightarrow \Lambda_c^+}$	-0.16 ± 0.02	--	0.35 ± 0.11
$g_1^{\Xi_{cc}^{++} \rightarrow \Lambda_c^+}$	0.09 ± 0.02	-0.22	-0.13 ± 0.08
$g_2^{\Xi_{cc}^{++} \rightarrow \Lambda_c^+}$	0.01 ± 0.00	0.05	0.037 ± 0.027
$g_3^{\Xi_{cc}^{++} \rightarrow \Lambda_c^+}$	-0.21 ± 0.02	--	0.31 ± 0.09
$f_1^{\Xi_{cc}^{++} \rightarrow \Sigma_c^+}$	-0.24 ± 0.01	-0.47	-0.35 ± 0.04
$f_2^{\Xi_{cc}^{++} \rightarrow \Sigma_c^+}$	-0.53 ± 0.05	1.04	1.15 ± 0.12
$f_3^{\Xi_{cc}^{++} \rightarrow \Sigma_c^+}$	0.03 ± 0.00	--	-1.40 ± 0.39
$g_1^{\Xi_{cc}^{++} \rightarrow \Sigma_c^+}$	-0.37 ± 0.05	-0.62	-0.23 ± 0.06
$g_2^{\Xi_{cc}^{++} \rightarrow \Sigma_c^+}$	-0.05 ± 0.00	0.05	-0.26 ± 0.15
$g_3^{\Xi_{cc}^{++} \rightarrow \Sigma_c^+}$	0.89 ± 0.06	--	2.68 ± 0.39

our form factors of $\Xi_{cc}^{++} \rightarrow \Lambda_c^+$ have an overall minus sign due to the convention on the baryon wave functions, which does not affect the physical quantities. Note that our results of the form factors at $q^2 = 0$ are significantly smaller than those in other approaches.

In FIGs. 3a and 3b, we compare the form factors of $\Xi_{cc}^{++} \rightarrow \Xi_c^+$ and $\Xi_{cc}^{++} \rightarrow \Lambda_c^+$, corresponding to $c \rightarrow s$ and $c \rightarrow d$ transitions, respectively. These form factors shall be identical

TABLE III: The form factors from the HBM with $\Xi_c^{(\prime)} = (\Xi_c^{(\prime)+}, \Xi_c^{(\prime)0})$ for $\Xi_{cc} = (\Xi_{cc}^{++}, \Xi_{cc}^+)$.

	$q^2 = 0$	$q^2 = q_{max}^2$		$q^2 = 0$	$q^2 = q_{max}^2$
$f_1^{\Xi_{cc} \rightarrow \Xi_c}$	0.45 ± 0.05	1.36 ± 0.00	$g_1^{\Xi_{cc} \rightarrow \Xi_c}$	0.14 ± 0.02	0.38 ± 0.00
$f_2^{\Xi_{cc} \rightarrow \Xi_c}$	-0.03 ± 0.00	-0.15 ± 0.01	$g_2^{\Xi_{cc} \rightarrow \Xi_c}$	0.01 ± 0.00	0.03 ± 0.01
$f_3^{\Xi_{cc} \rightarrow \Xi_c}$	-0.20 ± 0.04	-0.56 ± 0.03	$g_3^{\Xi_{cc} \rightarrow \Xi_c}$	-0.28 ± 0.04	-0.79 ± 0.02
$f_1^{\Xi_{cc} \rightarrow \Xi_c'}$	-0.31 ± 0.03	-0.70 ± 0.00	$g_1^{\Xi_{cc} \rightarrow \Xi_c'}$	-0.49 ± 0.04	-1.10 ± 0.01
$f_2^{\Xi_{cc} \rightarrow \Xi_c'^+}$	-0.63 ± 0.07	-1.48 ± 0.02	$g_2^{\Xi_{cc} \rightarrow \Xi_c'}$	-0.06 ± 0.02	-0.13 ± 0.02
$f_3^{\Xi_{cc} \rightarrow \Xi_c'^+}$	0.03 ± 0.01	0.06 ± 0.02	$g_3^{\Xi_{cc} \rightarrow \Xi_c'}$	1.00 ± 0.12	2.31 ± 0.05
$f_1^{\Omega_{cc}^+ \rightarrow \Omega_c^0}$	-0.48 ± 0.04	-0.99 ± 0.00	$g_1^{\Omega_{cc}^+ \rightarrow \Omega_c^0}$	-0.69 ± 0.06	-1.56 ± 0.02
$f_2^{\Omega_{cc}^+ \rightarrow \Omega_c^0}$	-0.93 ± 0.10	-2.17 ± 0.03	$g_2^{\Omega_{cc}^+ \rightarrow \Omega_c^0}$	-0.09 ± 0.02	-0.20 ± 0.04
$f_3^{\Omega_{cc}^+ \rightarrow \Omega_c^0}$	0.05 ± 0.02	0.11 ± 0.02	$g_3^{\Omega_{cc}^+ \rightarrow \Omega_c^0}$	1.52 ± 0.18	3.51 ± 0.08
$f_1^{\Xi_{cc}^{++} \rightarrow \Lambda_c^+}$	0.28 ± 0.05	1.42 ± 0.02	$g_1^{\Xi_{cc}^{++} \rightarrow \Lambda_c^+}$	0.09 ± 0.02	0.37 ± 0.00
$f_2^{\Xi_{cc}^{++} \rightarrow \Lambda_c^+}$	-0.01 ± 0.01	-0.16 ± 0.01	$g_2^{\Xi_{cc}^{++} \rightarrow \Lambda_c^+}$	0.01 ± 0.00	0.02 ± 0.01
$f_3^{\Xi_{cc}^{++} \rightarrow \Lambda_c^+}$	-0.16 ± 0.02	-0.73 ± 0.06	$g_3^{\Xi_{cc}^{++} \rightarrow \Lambda_c^+}$	-0.21 ± 0.02	-0.91 ± 0.05
$f_1^{\Omega_{cc}^+ \rightarrow \Xi_c^0}$	0.33 ± 0.05	1.41 ± 0.02	$g_1^{\Omega_{cc}^+ \rightarrow \Xi_c^0}$	0.10 ± 0.02	0.37 ± 0.00
$f_2^{\Omega_{cc}^+ \rightarrow \Xi_c^0}$	-0.01 ± 0.01	-0.11 ± 0.02	$g_2^{\Omega_{cc}^+ \rightarrow \Xi_c^0}$	0.01 ± 0.00	0.04 ± 0.01
$f_3^{\Omega_{cc}^+ \rightarrow \Xi_c^0}$	-0.20 ± 0.02	-0.75 ± 0.06	$g_3^{\Omega_{cc}^+ \rightarrow \Xi_c^0}$	-0.26 ± 0.03	-0.99 ± 0.06
$f_1^{\Xi_{cc}^{++} \rightarrow \Sigma_c^+}$	-0.24 ± 0.01	-0.70 ± 0.00	$g_1^{\Xi_{cc}^{++} \rightarrow \Sigma_c^+}$	-0.37 ± 0.05	-1.08 ± 0.01
$f_2^{\Xi_{cc}^{++} \rightarrow \Sigma_c^+}$	-0.53 ± 0.05	-1.65 ± 0.7	$g_2^{\Xi_{cc}^{++} \rightarrow \Sigma_c^+}$	-0.05 ± 0.00	-0.16 ± 0.03
$f_3^{\Xi_{cc}^{++} \rightarrow \Sigma_c^+}$	0.03 ± 0.00	0.09 ± 0.02	$g_3^{\Xi_{cc}^{++} \rightarrow \Sigma_c^+}$	0.89 ± 0.06	2.71 ± 0.16
$f_1^{\Omega_{cc}^+ \rightarrow \Xi_c^0}$	-0.24 ± 0.03	-0.70 ± 0.01	$g_1^{\Omega_{cc}^+ \rightarrow \Xi_c^0}$	-0.37 ± 0.05	-1.08 ± 0.01
$f_2^{\Omega_{cc}^+ \rightarrow \Xi_c^0}$	-0.56 ± 0.05	-1.71 ± 0.07	$g_2^{\Omega_{cc}^+ \rightarrow \Xi_c^0}$	-0.06 ± 0.00	-0.17 ± 0.03
$f_3^{\Omega_{cc}^+ \rightarrow \Xi_c^0}$	0.04 ± 0.00	0.11 ± 0.02	$g_3^{\Omega_{cc}^+ \rightarrow \Xi_c^0}$	0.97 ± 0.07	2.92 ± 0.18
$f_1^{\Xi_{cc}^+ \rightarrow \Sigma_c^0}$	-0.38 ± 0.05	-0.95 ± 0.03	$g_1^{\Xi_{cc}^+ \rightarrow \Sigma_c^0}$	-0.52 ± 0.07	-1.47 ± 0.05
$f_2^{\Xi_{cc}^+ \rightarrow \Sigma_c^0}$	-0.75 ± 0.07	-2.23 ± 0.00	$g_2^{\Xi_{cc}^+ \rightarrow \Sigma_c^0}$	-0.07 ± 0.00	-0.21 ± 0.03
$f_3^{\Xi_{cc}^+ \rightarrow \Sigma_c^0}$	0.05 ± 0.01	0.12 ± 0.03	$g_3^{\Xi_{cc}^+ \rightarrow \Sigma_c^0}$	1.26 ± 0.09	3.67 ± 0.07

in the limit of the $SU(3)_F$ symmetry. The figures show that for a fixed value of ω , the form factors are approximately the same. Explicitly, their values deviate by less than 13%. However, the phase space of the $c \rightarrow s$ transition is about 30% smaller than the one of $c \rightarrow d$. As shown in the figures, the form factors of $\Xi_{cc}^{++} \rightarrow \Xi_c^+$ with $\omega > 1.07$ are missing as they correspond to the region of $q^2 < 0$.

On the other hand, to examine the spectator effects, we plot the results of $\Xi_{cc}^{++} \rightarrow \Sigma_c^+$ and $\Omega_{cc}^+ \rightarrow \Xi_c^0$ in FIGs. 3c and 3d, corresponding to the $c \rightarrow d$ transition with (c, u) and (c, s) as the spectator quarks, respectively. We find that the form factors deviate less than

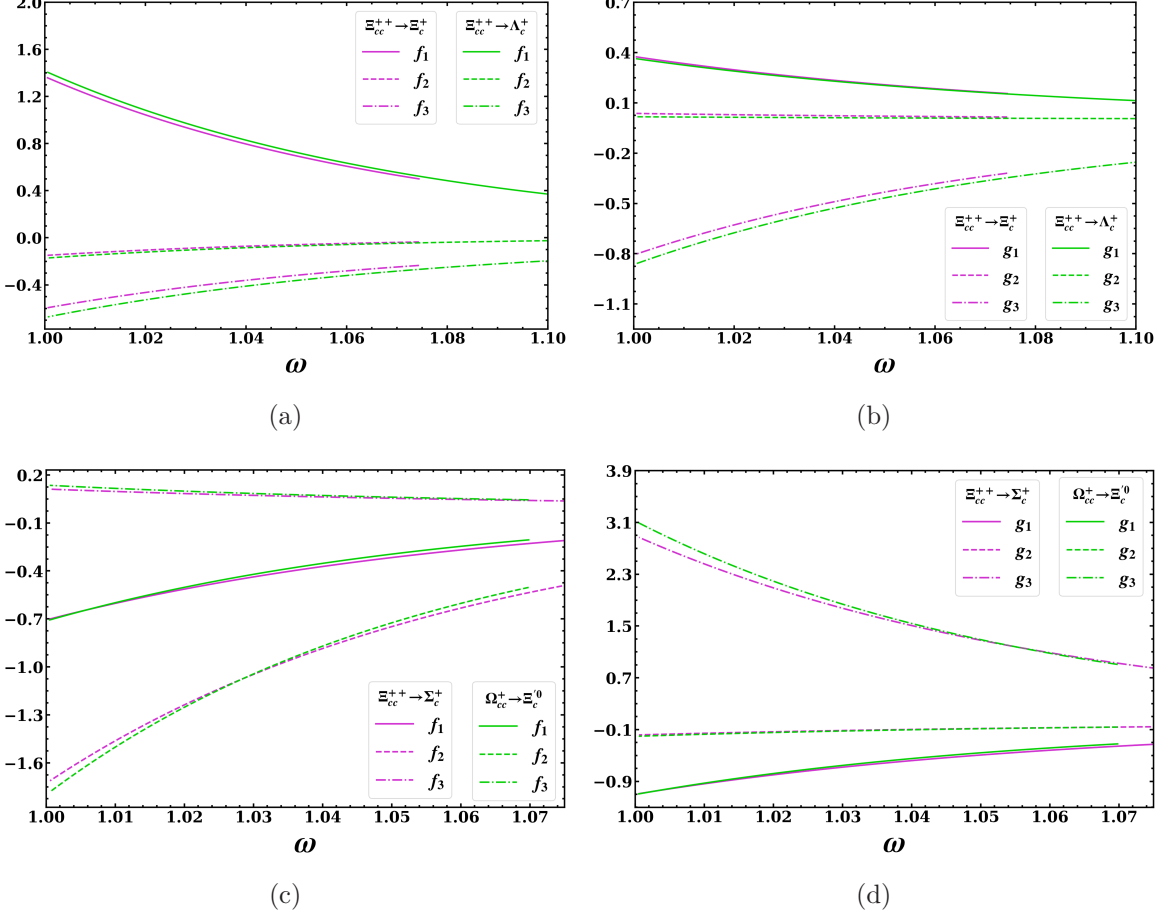


FIG. 3: The ω dependencies of the $B_{cc} \rightarrow B_c$ form factors.

11% between the two types of transition. We conclude that the form factors well respect the $SU(3)_F$ symmetry if one uses the variables of ω instead of q^2 .

The total decay widths of Γ are computed by integrating Eq. (6). To further examine the results, we decompose the decay widths into four fragments, given by

$$\begin{aligned}
 P_1 &= \frac{1}{\Gamma} \int_{m_e^2}^{\frac{1}{4}q_{max}^2} \partial_q \Gamma dq^2, & P_2 &= \frac{1}{\Gamma} \int_{\frac{1}{4}q_{max}^2}^{\frac{1}{2}q_{max}^2} \partial_q \Gamma dq^2, \\
 P_3 &= \frac{1}{\Gamma} \int_{\frac{1}{2}q_{max}^2}^{\frac{3}{4}q_{max}^2} \partial_q \Gamma dq^2, & P_4 &= \frac{1}{\Gamma} \int_{\frac{3}{4}q_{max}^2}^{q_{max}^2} \partial_q \Gamma dq^2,
 \end{aligned} \tag{16}$$

with their values listed in Table IV, respectively. The uncertainties of P_i are tiny compared to the total branching fractions due to the correlations. In addition, we find that except for $\Xi_{cc}^{++} \rightarrow \Xi_c^+ e^+ \nu_e$, the values of P_1 are the smallest among the fragments. In contrast to the others, the decay width of $\Xi_{cc}^{++} \rightarrow \Xi_c^+ e^+ \nu_e$ distributes smoothly among the four regions.

In FIG. 4, we plot the differential decay widths. In the high q^2 areas, the uncertainties

TABLE IV: The total and fragmentary decay widths.

channels	$\Gamma \times 10^{14} \text{ GeV}^{-1}$	P_1	P_2	P_3	P_4
$\Xi_{cc}^{++} \rightarrow \Xi_c^+ e^+ \nu_e$	5.11 ± 0.64	0.25 ± 0.02	0.29 ± 0.01	0.29 ± 0.01	0.17 ± 0.02
$\Xi_{cc}^{++} \rightarrow \Xi_c'^+ e^+ \nu_e$	10.9 ± 0.8	0.14 ± 0.01	0.24 ± 0.01	0.33 ± 0.00	0.29 ± 0.02
$\Omega_{cc}^+ \rightarrow \Omega_c^0 e^+ \nu_e$	22.1 ± 1.6	0.14 ± 0.01	0.24 ± 0.01	0.33 ± 0.00	0.29 ± 0.02
$\Xi_{cc}^{++} \rightarrow \Lambda_c^+ e^+ \nu_e$	0.34 ± 0.06	0.17 ± 0.03	0.26 ± 0.01	0.32 ± 0.00	0.24 ± 0.04
$\Xi_{cc}^{++} \rightarrow \Sigma_c^+ e^+ \nu_e$	0.76 ± 0.06	0.12 ± 0.02	0.21 ± 0.01	0.34 ± 0.00	0.34 ± 0.03
$\Xi_{cc}^+ \rightarrow \Sigma_c^0 e^+ \nu_e$	1.52 ± 0.12	0.12 ± 0.02	0.21 ± 0.02	0.34 ± 0.00	0.34 ± 0.03

are minor since f_1 and g_1 have few errors, as explained at the beginning of this section. We see that $\partial_q \Gamma(\Xi_{cc}^{++} \rightarrow \Xi_c^+ e^+ \nu_e)$ is much smoother than the others. To see the underlying reason, we define the parity conserving and violating partial decay widths as

$$P_C \equiv \partial_q \Gamma(g_i = 0), \quad P_V \equiv \partial_q \Gamma(f_i = 0), \quad \partial_q \Gamma = P_C + P_V, \quad (17)$$

where in $P_{C(V)}$ we take $g_{1,2,3}(f_{1,2,3})$ as zero, corresponding to the parity conserving (violating) parts of the decay widths. We show $P_{C,V}(\Xi_{cc}^{++} \rightarrow \Xi_c^{(\prime)+})$ in FIG. 5.

We see that $P_{C,V}$ have very different behaviors. On the one hand, P_C contribute to Γ mostly in the low q^2 regions, and their values decrease quickly as q^2 goes up. On the other hand, P_V behave oppositely. In $\Xi_{cc}^+ \rightarrow \Xi_c^+ e^+ \nu_e$, the net result is that the tendencies of $P_{C,V}$ smear out each other in $\partial_q \Gamma$. In contrast, the behavior of $\partial_q \Gamma$ is dominated by P_V in $\Xi_{cc}^{++} \rightarrow \Xi_c'^+ e^+ \nu_e$. The sharp difference can be traced back to the spin-flavor overlappings, where we approximately have $P_C \propto N_{\text{unflip}}^2$ and $P_V \propto N_{\text{flip}}^2$. From TABLE I, we see that $(N_{\text{flip}}/N_{\text{unflip}})^2$ are 1/9 and 100/36 for $\Xi_{cc}^+ \rightarrow \Xi_c^+$ and $\Xi_{cc}^{++} \rightarrow \Xi_c'^+$, respectively, which explains the opposite behaviors.

To test the lepton universality in the future experiments, we provide the ratios of

$$\mathcal{R} = \Gamma(B_{cc} \rightarrow B_c \mu^+ \nu_\mu) / \Gamma(B_{cc} \rightarrow B_c e^+ \nu_e)$$

in Table V. Their values are close to but below 1. Clearly, if $\mathcal{R} > 1$ in the future experiment, it will be a signal of new physics.

To eliminate the uncertainties caused by V_{cf} , by defining

$$G_{B_c}^{B_{cc}} = \frac{1}{|V_{cf}|^2} \Gamma(B_{cc} \rightarrow B_c e^+ \nu_e), \quad (18)$$

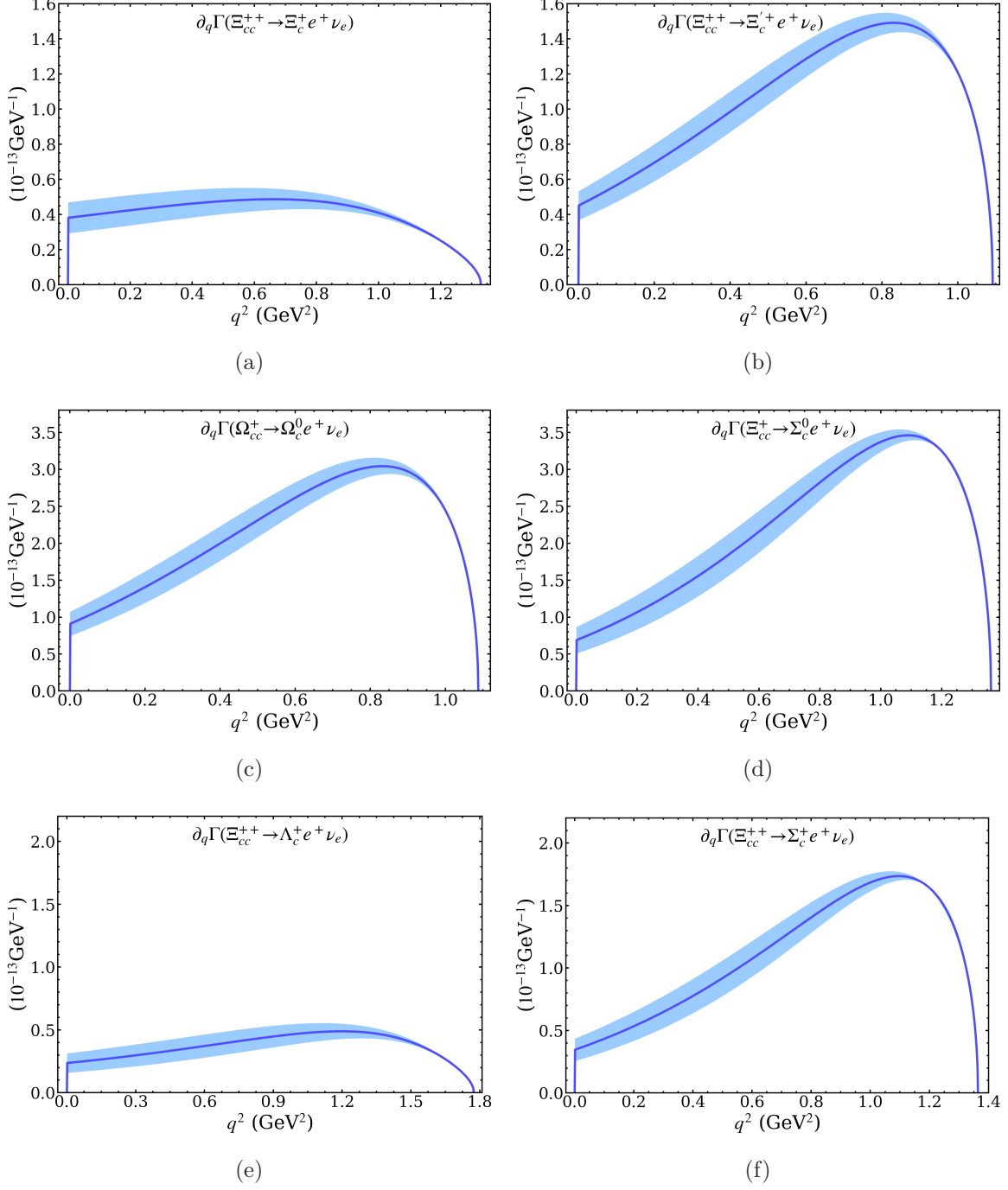


FIG. 4: The partial decay widths for $B_{cc} \rightarrow B_c e^+ \nu_e$, where the dashed lines and band widths are the center values and uncertainties, while (a, b, c) and (d, e, f) correspond to the $c \rightarrow s$ and $c \rightarrow d$ transitions, respectively.

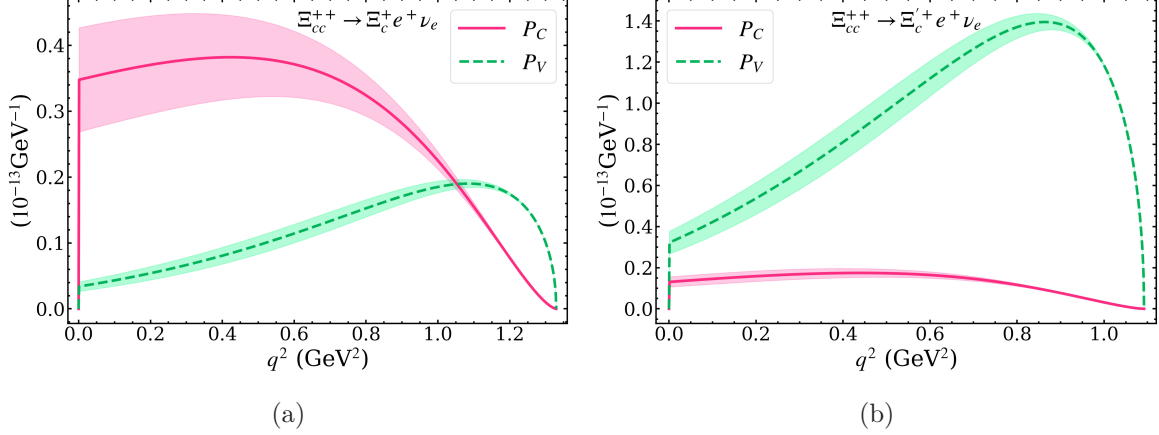


FIG. 5: The partial decay widths of P_C and P_V for $\Xi_{cc}^{++} \rightarrow \Xi_c^{(\prime)+} e^+ \nu_e$.

TABLE V: The ratios \mathcal{R} .

$c \rightarrow s$	\mathcal{R}	$c \rightarrow d$	\mathcal{R}
$\Xi_{cc}^{++} \rightarrow \Xi_c^+$	0.99	$\Xi_{cc}^{++} \rightarrow \Lambda_c^+$	1.00
$\Xi_{cc}^+ \rightarrow \Xi_c^0$	0.99	$\Omega_{cc}^+ \rightarrow \Xi_c^0$	1.00
$\Xi_{cc}^{++} \rightarrow \Xi_c^{\prime+}$	0.97	$\Xi_{cc}^{++} \rightarrow \Sigma_c^+$	0.97
$\Xi_{cc}^+ \rightarrow \Xi_c^{\prime0}$	0.97	$\Omega_{cc}^+ \rightarrow \Xi_c^{\prime0}$	0.97
$\Omega_{cc}^+ \rightarrow \Omega_c^0$	0.97	$\Xi_{cc}^+ \rightarrow \Sigma_c^0$	0.97

we find that

$$\begin{aligned}
 G_{\Xi_c^+}^{\Xi_{cc}^{++}} : G_{\Xi_c^0}^{\Xi_{cc}^+} : G_{\Lambda_c^+}^{\Xi_{cc}^{++}} : G_{\Xi_c^0}^{\Omega_{cc}^+} &= 1 : 0.99 : 1.24 : 1.17, \\
 G_{\Xi_c^{\prime+}}^{\Xi_{cc}^{++}} : G_{\Xi_c^{\prime0}}^{\Xi_{cc}^+} : \frac{1}{2} G_{\Omega_c^0}^{\Omega_{cc}^+} : G_{\Sigma_c^+}^{\Xi_{cc}^{++}} : G_{\Xi_c^0}^{\Omega_{cc}^+} : \frac{1}{2} G_{\Sigma_c^0}^{\Xi_{cc}^+} &= 1 : 0.99 : 1.01 : 1.30 : 1.32 : 1.31,
 \end{aligned} \tag{19}$$

which are all expected to be 1 in the exact $SU(3)_F$ symmetry. As mentioned in the discussions of the form factors early, the main $SU(3)_F$ breaking effects come from the phase space difference. For instance, from FIG. 4, the phase space of $\Xi_{cc}^{++} \rightarrow \Lambda_c^+$ is 1.3 times larger than the one of $\Xi_{cc}^{++} \rightarrow \Xi_c^+$, which partly explains the ratios in Eq. (19).

The computed decay widths, along with those in the literature, are shown in Table VI, where Ref. [9] computes the form factors by the MBM, Ref. [10] analyzes the decays with the heavy quark spin symmetry (HQSS), Refs. [11, 39] adopt the LFQM with different sets of the parameter input, and Ref. [41] calculates the decay widths by the QCDSR. The decay width of $\Xi_{cc}^{++} \rightarrow \Xi_c^{(\prime)+} e^+ \nu_e$ is slightly larger than the one of $\Xi_{cc}^+ \rightarrow \Xi_c^{(\prime)0} e^+ \nu_e$ as $M_{\Xi_{cc}^{++}}$ is 2

TABLE VI: The decay widths in units of 10^{-14} GeV along with the ones in the literature.

$B_{cc} \rightarrow B_c e^+ \nu_e$	This work	MBM [9]	HQSS [10]	LFQM [11]	LFQM [39]	QCDSR [41]
$\Xi_{cc}^{++} \rightarrow \Xi_c^+ e^+ \nu_e$	5.11 ± 0.64	7.36	5.78	11.50	8.74	7.72 ± 3.70
$\Xi_{cc}^+ \rightarrow \Xi_c^0 e^+ \nu_e$	5.08 ± 0.64	7.36	5.73	11.40	8.63	7.72 ± 3.70
$\Xi_{cc}^{++} \rightarrow \Xi_c^{\prime+} e^+ \nu_e$	10.92 ± 0.81	17.56	9.64	12.80	14.30	5.31 ± 3.52
$\Xi_{cc}^+ \rightarrow \Xi_c^{\prime0} e^+ \nu_e$	10.85 ± 0.81	13.02	9.57	12.70	14.10	5.31 ± 3.52
$\Omega_{cc}^+ \rightarrow \Omega_c^0 e^+ \nu_e$	22.09 ± 1.63	26.76	18.61	25.50	28.00	12.50 ± 8.02
$\Xi_{cc}^{++} \rightarrow \Lambda_c^+ e^+ \nu_e$	0.34 ± 0.06	0.46	0.32	1.05	0.80	0.76 ± 0.37
$\Omega_{cc}^+ \rightarrow \Xi_c^0 e^+ \nu_e$	0.32 ± 0.04	0.46	0.27	0.81	0.59	0.61 ± 0.28
$\Xi_{cc}^{++} \rightarrow \Sigma_c^+ e^+ \nu_e$	0.76 ± 0.06	0.78	0.52	0.96	1.09	0.49 ± 0.29
$\Omega_{cc}^+ \rightarrow \Xi_c^{\prime0} e^+ \nu_e$	0.77 ± 0.06	0.91	0.49	0.93	1.03	0.56 ± 0.35
$\Xi_{cc}^+ \rightarrow \Sigma_c^0 e^+ \nu_e$	1.52 ± 0.12	1.50	1.04	1.91	2.17	0.99 ± 0.58

MeV larger than $M_{\Xi_{cc}^+}$. For the $c \rightarrow s$ transition, our results of the decay widths are well consistent with the ones of the HQSS but systematically lower than those in the LFQM [39] and MBM [9] by a factor of 1.5. We note that in the MBM [9], the q^2 dependencies of the form factors are put by hand and independent of the spectator quarks. For instance, the q^2 dependencies of $\Lambda_c \rightarrow \Lambda$ and $\Xi_{cc}^{++} \rightarrow \Xi_c^+$ are taken to be the same in the MBM [9]. However, we emphasize that the spectator effects of the charm quark and others are very different, as shown explicitly in D_q^v of Eq. (8). The exponential factor of $\exp(-2iE_c v z)$ deviates largely to those of $\exp(-2iE_{u,d,s} v z)$. In particular, we find that it suppresses the decay widths by more than 40%, which causes the deviations between the results of the MBM and ours.

IV. CONCLUSION

We have studied the semileptonic decays of the doubly charmed baryons. Explicitly, we have found that $\Gamma(\Xi_{cc}^{++} \rightarrow \Xi_c^+ e^+ \nu_e, \Xi_c^{\prime+} e^+ \nu_e, \Lambda_c^+ e^+ \nu_e, \Omega_c^+ e^+ \nu_e) = (5.1 \pm 0.1, 11 \pm 1, 0.34 \pm 0.06, 0.76 \pm 0.06) \times 10^{-14}$ GeV, $\Gamma(\Xi_{cc}^+ \rightarrow \Xi_c^0 e^+ \nu_e, \Xi_c^{\prime0} e^+ \nu_e, \Sigma_c^0 e^+ \nu_e) = (5.1 \pm 0.6, 11 \pm 1, 1.5 \pm 0.1) \times 10^{-14}$ GeV, and $\Gamma(\Omega_{cc}^+ \rightarrow \Omega_c^0 e^+ \nu_e, \Xi_c^0 e^+ \nu_e, \Xi_c^{\prime0} e^+ \nu_e) = (22 \pm 2, 0.32 \pm 0.04, 0.77 \pm 0.06) \times 10^{-14}$ GeV. We have discussed the $SU(3)_F$ breaking effects regarding the aspects of (i) the phase spaces differences, (ii) the spectator quark effects, and (iii) the overlappings of the transited quarks. We have shown that the other breaking effects are negligible compared to

the phase space differences. In particular, the form factors well respect the $SU(3)_F$ relations using ω as the variables. In addition, we have obtained that $\Gamma(\Xi_{cc}^{++} \rightarrow \Lambda_c^+ e^+ \nu_e) V_{cs}^2 / \Gamma(\Xi_{cc}^{++} \rightarrow \Xi_c^+ e^+ \nu_e) V_{cd}^2 = 1.24$, which is expected to be 1 under the exact $SU(3)_F$ symmetry.

The behaviors of the parity violating and conserving partial decay widths have been examined. Accordingly, we have demonstrated that the partial decay width of $\Xi_{cc}^{++} \rightarrow \Xi_c^+ e^+ \nu_e$ is smoother than others, which can be testified in future experiments. We have also shown that the spectator effects of the charm quark suppress the decay widths by 40% and shall not be taken to be the same as the other quarks.

Acknowledgments

This work is supported in part by the National Key Research and Development Program of China under Grant No. 2020YFC2201501 and the National Natural Science Foundation of China (NSFC) under Grant No. 12147103.

-
- [1] M. Mattson *et al.* [SELEX], Phys. Rev. Lett. **89**, 112001 (2002).
 - [2] A. Ocherashvili *et al.* [SELEX], Phys. Lett. B **628**, 18 (2005).
 - [3] S. P. Ratti, Nucl. Phys. B Proc. Suppl. **115**, 33 (2003).
 - [4] B. Aubert *et al.* [BaBar], Phys. Rev. D **74**, 011103 (2006).
 - [5] Y. Kato *et al.* [Belle], Phys. Rev. D **89**, 052003 (2014).
 - [6] R. Aaij *et al.* [LHCb], Phys. Rev. Lett. **119**, 112001 (2017).
 - [7] R. Aaij *et al.* [LHCb], Phys. Rev. Lett. **121**, 052002 (2018).
 - [8] R. Aaij *et al.* [LHCb], Phys. Rev. Lett. **121**, 162002 (2018).
 - [9] R. Perez-Marcial, R. Huerta, A. Garcia and M. Avila-Aoki, Phys. Rev. D **40**, 2955 (1989).
 - [10] C. Albertus, E. Hernández and J. Nieves, Phys. Lett. B **704**, 499 (2011).
 - [11] W. Wang, F. S. Yu and Z. X. Zhao, Eur. Phys. J. C **77**, 781 (2017).
 - [12] L. Meng, N. Li and S. l. Zhu, Eur. Phys. J. A **54**, 143 (2018).
 - [13] W. Wang, Z. P. Xing and J. Xu, Eur. Phys. J. C **77**, 800 (2017).
 - [14] T. Gutsche, M. A. Ivanov, J. G. Körner and V. E. Lyubovitskij, Phys. Rev. D **96**, 054013 (2017).

- [15] H. S. Li, L. Meng, Z. W. Liu and S. L. Zhu, Phys. Lett. B **777**, 169 (2018).
- [16] Z. H. Guo, Phys. Rev. D **96**, 074004 (2017).
- [17] Q. F. Lü, K. L. Wang, L. Y. Xiao and X. H. Zhong, Phys. Rev. D **96**, 114006 (2017).
- [18] L. Y. Xiao, K. L. Wang, Q. f. Lu, X. H. Zhong and S. L. Zhu, Phys. Rev. D **96**, 094005 (2017).
- [19] N. Sharma and R. Dhir, Phys. Rev. D **96**, 113006 (2017).
- [20] Y. L. Ma and M. Harada, J. Phys. G **45**, 075006 (2018).
- [21] F. S. Yu, H. Y. Jiang, R. H. Li, C. D. Lü, W. Wang and Z. X. Zhao, Chin. Phys. C **42**, 051001 (2018).
- [22] L. Meng, H. S. Li, Z. W. Liu and S. L. Zhu, Eur. Phys. J. C **77**, 869 (2017).
- [23] X. H. Hu, Y. L. Shen, W. Wang and Z. X. Zhao, Chin. Phys. C **42**, 123102 (2018).
- [24] Y. J. Shi, W. Wang, Y. Xing and J. Xu, Eur. Phys. J. C **78**, 56 (2018).
- [25] L. Y. Xiao, Q. F. Lü and S. L. Zhu, Phys. Rev. D **97**, 074005 (2018).
- [26] D. L. Yao, Phys. Rev. D **97**, 034012 (2018).
- [27] U. Özdem, J. Phys. G **46**, 035003 (2019).
- [28] A. Ali, A. Y. Parkhomenko, Q. Qin and W. Wang, Phys. Lett. B **782**, 412 (2018).
- [29] J. M. Dias, V. R. Debastiani, J. J. Xie and E. Oset, Phys. Rev. D **98**, 094017 (2018).
- [30] R. H. Li and C. D. Lu, arXiv:1805.09064 [hep-ph].
- [31] R. Dhir and N. Sharma, Eur. Phys. J. C **78**, 743 (2018).
- [32] A. Cerri, V. V. Gligorov, S. Malvezzi, J. Martin Camalich, J. Zupan, S. Akar, J. Alimena, B. C. Allanach, W. Altmannshofer and L. Anderlini, *et al.* CERN Yellow Rep. Monogr. **7**, 867 (2019).
- [33] A. V. Berezhnoy, A. K. Likhoded and A. V. Luchinsky, Phys. Rev. D **98**, 113004 (2018).
- [34] L. J. Jiang, B. He and R. H. Li, Eur. Phys. J. C **78**, 961 (2018).
- [35] Q. A. Zhang, Eur. Phys. J. C **78**, 1024 (2018).
- [36] L. Meng and S. L. Zhu, Phys. Rev. D **100**, 014006 (2019).
- [37] T. Gutsche, M. A. Ivanov, J. G. Körner, V. E. Lyubovitskij and Z. Tyulemissov, Phys. Rev. D **99**, 056013 (2019).
- [38] X. H. Hu and Y. J. Shi, Eur. Phys. J. C **80**, 56 (2020).
- [39] X. H. Hu, R. H. Li and Z. P. Xing, Eur. Phys. J. C **80**, 320 (2020).
- [40] Y. J. Shi, Y. Xing and Z. X. Zhao, Eur. Phys. J. C **79**, 501 (2019).
- [41] Y. J. Shi, W. Wang and Z. X. Zhao, Eur. Phys. J. C **80**, 568 (2020).

- [42] Z. X. Zhao, Eur. Phys. J. C **78**, 756 (2018).
- [43] Y. Xing and R. Zhu, Phys. Rev. D **98**, 053005 (2018).
- [44] A. Ali, Q. Qin and W. Wang, Phys. Lett. B **785**, (2018).
- [45] M. Z. Liu, Y. Xiao and L. S. Geng, Phys. Rev. D **98**, 014040 (2018).
- [46] Z. P. Xing and Z. X. Zhao, Phys. Rev. D **98**, 056002 (2018).
- [47] R. Zhu, X. L. Han, Y. Ma and Z. J. Xiao, Eur. Phys. J. C **78**, 740 (2018).
- [48] C. Q. Geng, C. W. Liu and T. H. Tsai, Phys. Rev. D **102**, 034033 (2020).
- [49] C. W. Liu and C. Q. Geng, JHEP **01**, 128 (2022).
- [50] C. Q. Geng, X. N. Jin and C. W. Liu, Phys. Rev. D **106**, 053006 (2022).
- [51] C. Q. Geng, X. N. Jin and C. W. Liu, arXiv:2210.15588 [hep-ph].
- [52] J. Zhang, X. N. Jin, C. W. Liu and C. Q. Geng, arXiv:2210.16825 [hep-ph].
- [53] C. W. Liu and C. Q. Geng, arXiv:2205.08158 [hep-ph].
- [54] A. Kadeer, J. G. Korner and U. Moosbrugger, Eur. Phys. J. C **59**, 27 (2009).
- [55] C. Q. Geng, C. W. Liu, T. H. Tsai and S. W. Yeh, Phys. Lett. B **792**, 214 (2019).
- [56] J. G. Korner, M. Kramer and D. Pirjol, Prog. Part. Nucl. Phys. **33**, 787 (1994).
- [57] R. L. Workman *et al.* [Particle Data Group], PTEP **2022**, 083C01 (2022).
- [58] W. X. Zhang, H. Xu and D. Jia, Phys. Rev. D **104**, 114011 (2021).